5 Cloud and Precipitation Observed with Radar

Martin Hagen[1], Axel Häring[1], Stefan Kneifel[2], Kersten Schmidt[3]

Abstract

Meteorological radar is an essential tool for research, diagnosis, and nowcasting of clouds and precipitation. Cloud radars use short wavelengths to enable detection of small ice particles or cloud droplets. The cloud radar at UFS Schneefernerhaus is operated since end of 2011. It has been used for a number of studies related to clouds and precipitation. In a synergistic combination with additional remote sensing instruments, a large variety of cloud and precipitation properties can be retrieved. The measurements at UFS Schneefernerhaus can be used for the evaluation of numerical weather prediction models and satellite measurements. The long-term observations allow assessing the seasonal and long-term evolution of cloud properties above the UFS in a warming climate.

Key words: radar, clouds, precipitation

5.1 Introduction

Clouds and precipitation play an important role in the atmosphere. Clouds do contribute considerable to the uncertainty of future climate predictions. Depending on the height and vertical extent, they contribute differently on the warming or cooling of the Earth surface. Clouds have also an essential impact on the local radiation budget and thus controlling the local climate. Cloud particles can grow to precipitation in the form of rain, snow, graupel, or hail. This has a direct impact on the local water budget.

While in-situ measurements (c. f. Chapter 22: Impact of turbulence on cloud micrphysics) can describe the internal structure of clouds at a specific point in great detail, remote sensing techniques give more insights into the two- or three-dimensional variability. Optical methods (c. f. Chapter 18 and 21) are very suitable for optically thin clouds; however, radar is able to penetrate also clouds and even strong precipitation and thus, complements the optical observations in an optimal way.

Different types of meteorological radar systems are available and used for various purposes. Weather radars are mainly used by meteorological services for identification, monitoring and tracking of precipitation systems like frontal systems or thunderstorms. Short-term weather forecast is often done by tracking radar echoes and extrapolating their motion. The surveillance range is a few hundred kilometers. Fast scanning antennas and powerful signal processing allows high temporal (2–10 minutes) and spatial (50–1000 m) resolution of the volumetric measurement of precipitation systems. Weather radars use centimeter wavelengths because the signal is only weakly attenuated by even heavy precipitation, thus, allowing to receive information up to 300 km away from the radar. For the detection of non-precipitating clouds – where the typical particle size is in the order of 10 to 100 µm – cloud radars with a wavelength in the millimeter range are used. Those systems have limited measurement range up to 10 or 30 km, their antennas are either pointing vertically only, or able to scan but with a much slower scanning rate than what is used for weather radar.

At Umweltforschungsstation Schneefernerhaus (UFS), two vertically looking radar systems are permanently installed: a cloud radar and a micro rain radar with a wavelength of 0.8 cm and 1.2 cm, respectively. This contribution mainly focuses on cloud radars and their application with emphasis on the system operated at UFS.

[1] Deutsches Zentrum für Luft- und Raumfahrt, Institut für Physik der Atmosphäre
[2] Universität zu Köln, Institut für Geophysik und Meteorologie
[3] Deutsches Zentrum für Luft- und Raumfahrt, Institut für Hochfrequenztechnik und Radarsysteme

5

5.2 Radar Principles

5.2.1 Radar Techniques

A radar transmits a short electromagnetic pulse with high power through a directional antenna. This pulse is reflected by an object and received by the radar receiver (c. f. Fig. 1). The direction in which the antenna is pointed and the round-trip time of the pulse are used to locate the object which is scattering the pulse. The principal components of a weather radar are the transmitter, the antenna, the receiver, the signal processor, and the product and image generator. The transmit/receive switch and/or limiter is needed to protect the sensitive receiver from the high power transmit pulse. Radar operation control, signal processing, and image generation is accomplished with powerful standard computers. Here, only a basic overview of radar systems can be provided. More details on meteorological radars can be found in textbooks like Fabry (2015) or Bringi and Chandrasekar (2001). Radar techniques are described in detail in Skolnik (2008).

In the following, some technical aspects of meteorological radars will be described. The weather radar is mentioned for completeness, the focus will be on the two radar systems – namely a cloud radar and a micro-rain-radar – operated for research at the Umweltforschungsstation Schneefernerhaus. Table 1 summarizes some technical characteristics of typical weather radar used in Europe and the two systems operated at UFS.

5.2.1.1 Weather Radar

Weather radars are used for a wide spectrum of operational applications such as:

- identifying precipitation systems (like fronts or thunderstorms) for weather prediction,
- detailed analysis of dynamical and microphysical structures in thunderstorms,
- monitoring thunderstorm motion for nowcasting,
- estimating precipitation amount for hydrological applications like flood forecasting for river catchments,
- identifying of thunderstorm or hail swaths,
- long term observations for precipitation climatologies.

The main focus of weather radar is on precipitating particles like rain, snow, graupel or hail, for this purpose long wavelengths are suited best. A total number of about 200 weather radars are operated by meteorological services in Europe today. Most weather radars in Europe are C-band radars (frequency 5.6 GHz, wavelength 5.4 cm); only some radars in the Mediterranean area are S-band radars (frequency 2.8 GHz, wavelength 10.7 cm). X-band radars (9.4 GHz, wavelength 3.2 cm) are used for research applications and short range observations like cities or river catchments, but also in mountainous regions to cover valleys which are shielded from the long-range radars located outside the mountains or on mountain peaks.

Besides measuring the strength of the backscattered signal (termed as reflectivity; c. f. section 5.2.2.1), weather radars can measure the motion of the scattering particles (c. f. section 5.2.2.2). Dual-polarization capabilities enable the estimation of the particle properties and the classification of hydrometeors (c. f. section 5.2.2.4, 5.2.2.5, and Bringi and Chandrasekar (2001)).

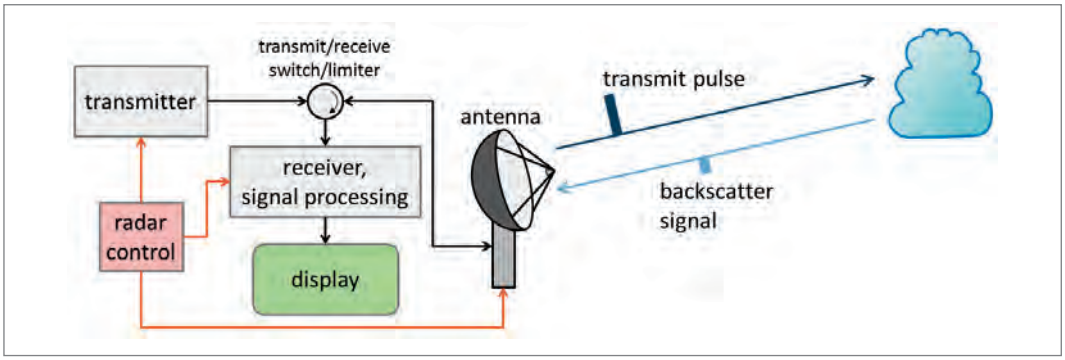

Fig. 1: Principle of meteorological radar.

Tab. 1: Characteristics of typical European weather radar, as well as of the cloud radar and the micro-rain-radar installed at Umweltforschungsstation Schneefernerhaus.

Parameter	Typical weather radar	MIRA36 cloud radar	MRR micro rain radar
Frequency band	C-band	Ka-band	K-band
Frequency/wavelength	5.6 GHz / 5.4 cm	35.5 GHz / 0.8 cm	24.1 GHz / 1.2 cm
Transmit power	500 kW (pulse peak)	25 kW (pulse peak)	50 mW (continuous wave)
Pulse duration	0.6–2 µs	0.2 µs	frequency modulated – continuous wave
Pulse repetition frequency	500–1200 Hz	5000 Hz	frequency modulated – continuous wave
Integration time per sample	0.02–0.1 s	10 s	60 s
Depth of measurement volume	90–300 m	30 m	50–100 m
Maximum range	100–300 km	15 km	1.5–3 km
Antenna diameter	4 m	1 m	0.6 m
Antenna rotation speed	2–6 rpm	fixed vertical pointing	fixed vertical pointing
Half-power beam width	1°	0.6°	2°

5.2.1.2 Cloud Radar

Cloud radars are designed for the observation of small cloud particles. For that purpose, radars with short wavelengths are used (Ka- or W-band; frequency 35 or 95 GHz; wavelength 8 or 3 mm, respectively). By using shorter wavelengths, the sensitivity to smaller particles, such as cloud droplets or tiny ice particles, increases. However, the backscattered signal also gets increasingly attenuated by hydrometeors and atmospheric gases which limits the maximum range that can be probed with the radar. Most of the cloud radars use vertically pointing antennas, only a few cloud radars are able to scan the hemisphere. Even though a variety of cloud radars does exist, this chapter is focused on the vertical pointing MIRA36 cloud radar installed at UFS and manufactured by METEK GmbH (e.g. Görsdorf et al., 2015). This radar system is characterized by high transmit power and its sensitivity to low backscatter signals. A number of MIRA36 systems are available worldwide. At the Meteorological Institute of Ludwig-Maximilians-Universität at Munich a MIRA36 radar with scanning capabilities is installed. A downward looking MIRA36 (Mech et al., 2014) is available to be flown onboard the German research aircraft HALO (High Altitude and Long-range) during specific campaigns.

Fig. 2: Installation of the MIRA36 cloud radar at Umweltforschungsstation Schneefernerhaus. Left: antenna of Casegrain type during the installation phase with parabolic dish, feed horn in the center and sub-reflector at the top. Center: antenna with clutter fence. Right: radar transmitter and receiver within the suspended ceiling of Wechselnutzerlabor. Photos by M. Hagen.

Fig. 3: Installation of the PARSIVEL-2 disdrometer (left) and MRR micro rain radar (right) at the top terrace of the Umweltforschungsstation Schneefernerhaus. Photo by M. Hagen.

During the TOSCA campaign (c. f. section 5.3.3 and Löhnert et al., 2011) in 2008/2009 a MIRA36 cloud radar was temporally installed at the terrace at UFS. With the experience collected during TOSCA and the added value generated by its combination with other remote sensing instrumentation at UFS, a permanent installation of a MIRA36 cloud radar was planned and realized in the end of 2011. The antenna of the cloud radar is mounted at the roof of the 5th floor (Fig. 2, left), the radar electronics and computers are installed within the suspended ceiling of the *Wechselnutzerlabor* at the 5th floor (Fig. 2, right). Radar control and support (uninterrupted power supply and dry air compressor) are installed in a computer rack at the *Wechselnutzerlabor*. The antenna is surrounded by a clutter fence (Fig. 2, middle) to prevent interference of the radar beam with the building and the mountains of the Zugspitzgrad. The radar has been operated continuously since December 2011. Due to maintenances and other technical issues, occasionally interruptions of the operation do occur.

The primary measurement quantity of the MIRA36 cloud radar is the Doppler spectrum (c. f. section 5.2.2.3), from which common moments or radar parameters such as reflectivity or Doppler velocity can are derived (c. f. section 5.2.2). Both, the Doppler spectra themselves and the moments, are stored for long-term access. Doppler spectra provide detailed information on the vertical motion of the particles. Under the assumption that there is no vertical air motion, information on the particle habit can be retrieved (e. g. Kollias et al., 2011). More detailed analysis of the spectra also allow to separate different hydrometeor classes (e. g. Melchionna et al., 2008). The polarization capabilities allow for the discrimination of spherical water drops, irregular shaped ice crystals, melting particles, as well as insects.

5.2.1.3 Micro Rain Radar

The micro rain radar (MRR) manufactured by METEK GmbH (e. g. Peters et al., 2002) is a low-cost radar designed for the estimation of vertical profiles of raindrop size distributions. Since the radar is using low-power electronics and is using the frequency-modulated continuous-wave (FM-CW) principle, it is a very robust system. A MRR is operated at the Umweltforschungsstation Schneefernerhaus since January 2008 on top of the building (Fig. 3). For the estimation of the in-situ raindrop size distribution, it is accompanied by an optical disdrometer PARSIVEL-2 (Löffler-Mang and Joss, 2000) manufactured by OTT-Hydromet GmbH. The disdrometer provides spectral particle size distribution and spectral fall-velocity distribution which can be used to classify the kind of precipitation (e. g., snow, rain, hail). Both instruments, the MRR and PARSIVEL-2, are designed for the observation of precipitating particles (raindrops, snowflakes or aggregates, graupel, hail); their sensitivity is not sufficient to observe cloud particles like cloud droplets or ice needles, plates, or dendrites.

The standard retrieval of raindrop size distributions provided by the manufacturer assumes a stagnant vertical air motion. The basic principle of this raindrop size distribution retrieval is shortly summarized in the following: within the Doppler spectra, each velocity bin (i. e. fall speed of raindrops) can be related to the associated raindrop size via known fall speed – drop size relations (e. g. Atlas et al., 1973). In a next step, the backscatter cross section for a single

drop of this size is estimated using Mie scattering theory. The measured spectral power at the relevant velocity bin is then simply divided by the known backscatter power for a single drop in order to obtain the number of drops for that size.

Even though the MRR has a lower sensitivity compared to the high power and high sensitive cloud radar, both instruments show good agreement over a wide range of precipitation intensity and with appropriate processing snow parameters can be derived (Kneifel et al., 2011). Due to the parallel operation of MIRA and MRR at UFS, the retrieval algorithms have been further developed to also enable the remote sensing community to measure snowfall with the MRR (Maahn and Kollias, 2012). Further evaluation of precipitation measurements by MRR are shown in Kneifel et al. 2022.

5.2.2 Radar Parameters

Air traffic control, military radars or ship radars aim detecting point targets. With meteorological radars, multiple targets filling the radar volume, such as rain or snow, shall not only be detected but also quantified. While conventional weather radars measure only the intensity of the returned signal, a Doppler radar additionally estimates the motion of the target. This provides for example information about the wind field but also allows to precisely monitor the motion of a thunderstorm. A further extension of Doppler radars is the addition of polarization which allows to derive a number of valuable additional radar parameters. Since dual-polarization radar use electromagnetic waves with two orthogonal polarizations, the derived radar parameters allow a characterization of the shape and orientation of the target. More details about the various radar parameters can be found in text books like Fabry (2015) or Bringi and Chandrasekar (2001).

5.2.2.1 Radar Reflectivity Factor

Radar reflectivity is a synonym for the magnitude of the reflected radar pulse. The radar equation for volume targets gives the relationship between the received signal P_r and the scattering cross section σ of the target

$$P_r = \frac{P_t g^2 \lambda^2}{64 \pi^3 r^4} \frac{\pi r^2 \theta_0^2 h}{8} \frac{1}{2 \ln(2)} \sum_{i=1}^{n} \sigma_i \tag{1}$$

with P_t the transmitted power, g the antenna gain, λ the wavelength, θ_0 the beam width, h the pulse length, r the distance to the targets, and σ_i the scattering cross section of the individual targets within volume. It is assumed that the measurement volume is uniformly filled with scattering targets. The first term describes the received power for a single point target, the second term the measurement volume, and the third term accounts for the fact that only part of the transmitted power is within the measurement volume bounded by the half-power beam width θ_0.

For particles which are large compared to the wavelength (diameter $D > 10\ \lambda$), the scattering cross section σ of a target is similar to its geometric cross section. For particles much smaller than the wavelength ($D < 1/10\ \lambda$), the scattering cross section can be approximated by Rayleigh scattering

$$\sigma = \frac{\pi^5}{\lambda^4} |K|^2 D^6 \tag{2}$$

with $K = (m^2 - 1)/(m^2 + 2)$ representing the complex refractive index m of the scattering particle ($|K|^2 \approx 0.93$ for water and $|K|^2 \approx 0.2$ for ice). With the assumption that the targets are liquid water particles and much smaller than the wavelength, the radar reflectivity factor[4] z is defined as the sum of D^6 of all particles within the unit volume V

$$z = \frac{1}{V} \sum_{i=1}^{n} D_i^6 \tag{3}$$

The common unit of z is mm^6/m^3. Electrical engineers usually express a ratio R of two powers (p_1 and p_2) in a logarithmic notation $R = 10 \log_{10}(p_1/p_2)$. The "unit" of such a ratio is the decibel (dB). It is common in radar meteorology to express the reflectivity factor as a logarithmic ratio with respect to the reflectivity factor of a raindrop with a diameter of 1 mm.

[4] Informally, but also in a large number of publications, the term "reflectivity" is used instead of "reflectivity factor."

$$Z = 10 \log\left(\frac{z}{1\ \mathrm{mm}^6\,\mathrm{m}^{-3}}\right) \tag{4}$$

The unit of the logarithmic quantity Z is termed dBz (decibel z).

5.2.2.2 Doppler Velocity and Spectral Width

If a relative motion does exist between the radar and the target, a frequency shift of the reflected wave can be observed by the radar. This effect was first described by the Austrian astronomer Christian Doppler in 1842. The resulting frequency is given by $f = f_0(1 \pm v/c)$ with f_0 the transmitted frequency, v the relative speed and c the propagation speed of the wave (speed of light). The difference $(f - f_0)$ is defined as the Doppler frequency f_D. In the case of radar the frequency shift is doubled, since the Doppler Effect occurs twice, once on the way to the target and once on the way back to the radar

$$f_D = \pm \frac{2v}{\lambda} \tag{5}$$

Due to technical limitations, the radar cannot measure the Doppler frequency directly; instead the radar detects phase differences between a number (~20 to ~250) of radar pulses and determines the Doppler frequency and its standard deviation from a time series of phase measurements. Even though radar doesn't measure the frequency shift directly, in radar meteorology the term Doppler velocity[5] is widely used. Only a motion towards or away from the radar (the radial or line-of-sight component) can be detected by the Doppler Effect. By convention, a motion towards the radar introduces a negative Doppler velocity and a motion away from the radar a positive Doppler velocity. In general, it is assumed that precipitation particles move with the wind; however, their fall speed has to be taken into account. For vertical pointing radars, the observed Doppler velocity is the superposition of vertical air motion and fall speed of the particles.

The standard deviation of the phase measurements is termed spectral width because it describes the width of the Doppler velocity spectrum. Spectral width is a measure of the turbulence within the measurement volume – or – in the case of vertical pointing radar a measure of the diverse fall speed of different particle types and sizes.

5.2.2.3 Doppler Spectrum

Besides the technique described above, the phase measurements can be transferred by a Fourier transformation into frequency domain. Frequency is equivalent to Doppler velocity in this case (c. f. Eq. 5). The Doppler spectrum gives the backscattered power or reflectivity for each Doppler velocity bin. Fig. 4 shows an example of a Doppler spectrum from the vertical pointing MIRA36 cloud radar at UFS. The green area is the signal-to-noise ratio (SNR) of this spectrum

[5] In radar meteorology the term "radial" component or velocity is preferred; scientists working with lidar prefer the term "line-of-sight" component or velocity.

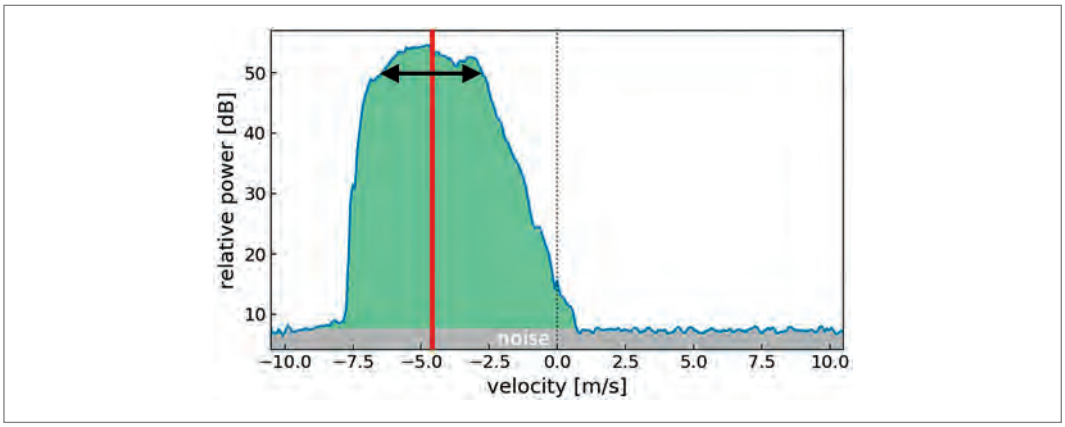

Fig. 4: Doppler spectrum (blue line) measured with MIRA36 at UFS (21 July 2018, 05:24 UTC, 300 m AGL). Grey area indicates noise level, green area is signal-to-noise power, red line is mean Doppler velocity, and black line with arrows indicates spectral width.

after the noise has been subtracted (in dB). With appropriate radar calibration constants, reflectivity can be derived from the measured SNR. Mean Doppler velocity is indicated by the red vertical line and the horizontal line with arrows indicate the estimation of the spectral width.

For the microphysical retrieval of observed clouds, several methods for evaluating Doppler spectra were developed, e. g. fitting of multi-modal Gauss curves (Melchionna et al., 2008) or determining of third (skewness) and fourth (kurtosis) moment of the spectrum to predict the onset of drizzle inside liquid clouds (Kollias et al., 2011; or Acquistapace et al., 2017).

5.2.2.4 Differential Reflectivity

Common dual-polarization weather radars use linear polarization with horizontal and vertical polarization planes. Differential reflectivity (Z_{DR}) is the ratio between the reflectivity factor measured at horizontal and vertical polarization

$$Z_{DR} = 10 \log \left(\frac{z_H}{z_V} \right) \tag{6}$$

with z_H the reflectivity factor at horizontal polarization and z_V the reflectivity factor at vertical polarization (both in mm^6/m^3). The unit of Z_{DR} is dB. Z_{DR} is the standard radar parameter, which can be measured with dual-polarization radar. Positive Z_{DR} is observed when particles are flat and fall more horizontally aligned. This is the case for raindrops larger than 1 mm in diameter and for ice needles or plates. Z_{DR} is used to improve the rainfall rate estimation and to identify hydrometeors. For measurements at low elevation angles, the range of Z_{DR} in rain is 0–5 dB. Particles like graupel or hail have an irregular shape and tumble and rotate during descent. Their Z_{DR} is typically around zero. For vertically pointing cloud radars this parameter is normally not used since particles fall horizontal aligned and due to their random horizontal orientation, no difference between the two orthogonal polarizations is observed.

5.2.2.5 Linear Depolarization Ratio

The linear depolarization ratio (*LDR*) describes how much energy of the transmitted horizontal polarized wave is scattered back vertically polarized

$$LDR = 10 \log \left(\frac{z_{VH}}{z_H} \right) \tag{7}$$

with z_{VH} the reflectivity factor (in mm^6/m^3) received with vertical polarization while transmitted with horizontal polarization. The unit of *LDR* is dB. *LDR* is caused by particles which are canted during falling or tumble and rotate heavily while falling. These are usually particles which have an irregular shape and/or are water coated ice particles like melting snowflakes or wet graupel or hail. *LDR* is about –35 dB in weak rain, –25 dB for graupel and –15 dB or higher for melting hail. *LDR* is also used to classify hydrometeors and to detect the presence of insects (frequently observed also at UFS). The lower limit of *LDR* is given by technical constraints like the isolation between the two receiver channels and the purity of the antenna shape and the feed horn.

5.3 Observations and Measurements at UFS

5.3.1 Clouds and Precipitation

5.3.1.1 Cloud Statistics

The continuous operation of the cloud radar since December 2011 allows for the evaluation of statistical properties of clouds and precipitation in the Alpine region above the Schneefernerhaus. An exemplary analysis is shown in Fig. 5, more detailed analysis can be found in Häring (2016). Kneifel et al., 2022 present a statistical analysis of clouds and precipitation at UFS by combining radar with other long-term remote sensing observations available at UFS.

Fig. 5 shows the frequency distribution of reflectivity and Doppler velocity as well as the normalized number of observations with height for the year 2014. The radar is located at 2671 m above sea level. For the first 150 or 180 m above the radar, no radar measurements are available since the radar has to switch from transmit to receive which requires a finite amount of time.

5

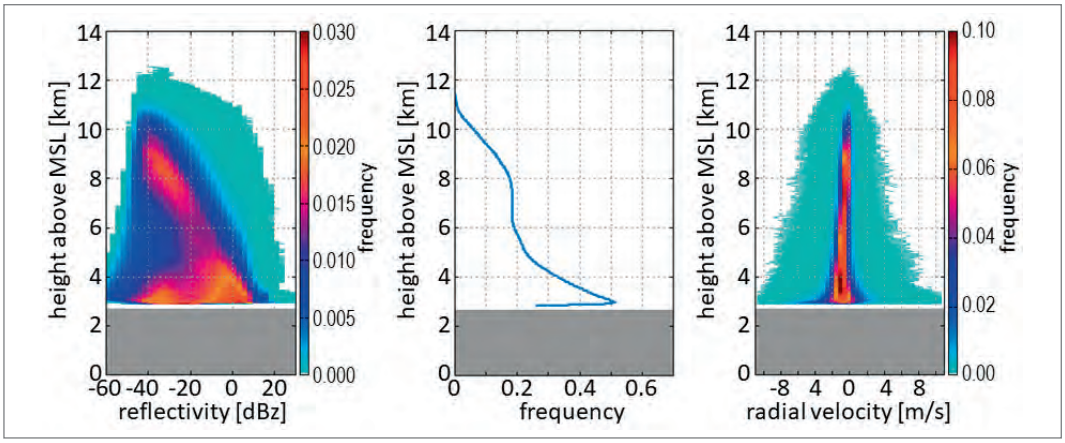

Fig. 5: Frequency distribution of reflectivity as a function of height (left), normalized number of reflectivity observations (center), and frequency distribution of Doppler velocity (right) for the year 2014.

An automatic quality control and hydrometeor classification was used to filter meteorological echoes from non-meteorological echoes like ground targets, birds, insects, or the gondola of the *Gletscherbahn*.

Fig. 5 (center) shows that about half of the time there are low clouds above Schneefernerhaus or the site itself is within clouds. The fraction is decreasing with height due to the variation in thickness of clouds. At about 20 % of the time there are clouds in the height band 6 to 8 km above sea level. These are cirrus clouds with varying thickness. Clouds reach up to 12.5 km MSL.

The frequency of reflectivity measurements (Fig. 5, left) shows a wide range reaching from about 20 dBz down to the minimum sensitivity of the radar which is about –50 dBz at a range of 5 km from the radar. Three distinct maxima can be identified in the reflectivity distribution: The maximum around 8 km height indicates reflectivity values of cirrus clouds, the rare occurrence of high values at that height are related to deep convection. At low levels two maxima can be identified. The one at high reflectivity values is related to precipitation, the other at low reflectivity values is related to clouds. The high reflectivity values below 3.5 km indicate the occurrence of rain during summer. The growths of particles from cloud to precipitation can be seen with the increase of the reflectivity center with decreasing height.

The frequency distribution of Doppler velocity (Fig. 5, right) shows a wide range of observed velocities. While the fall speed (i. e. negative Doppler velocity) of cloud particles is in the order of 0.1 m/s, the typical fall velocity of snow is 1 m/s, and of rain is about 5 m/s; the observations show a broad distribution around the expected values. The reason for this is vertical air motion caused by the flow over the Alps and leading to strong up- and downdrafts. An example is shown in the next section.

5.3.1.2 Case Studies

Three exemplary observations typical for the cloud radar measurements at Schneefernerhaus will be shown in this section.

The first example contains observations of contrail cirrus. Fig. 6 shows the visual impression taken with a vertical looking camera and the associated reflectivity observations with the cloud radar. The reflectivity time-height display shows at least three structures which can be attributed to contrail cirrus, namely at 15:05, 15:20 and 15:30 UTC on March 3rd, 2015. The contrail cirrus forms first at about 3.9 km above the radar and then descent during about 3–4 minutes down to 3.3 km. Below that height, obviously ambient humidity is too low and the contrails dissolve rapidly. The cloud layer at about the same height later on indicates that the atmosphere was sufficiently humid for contrail formation. The very thin cloud layer between 15:15 and 15:30 is hardly to be seen in the photo.

Fig. 7 shows time-height cross-sections of reflectivity and Doppler velocity of a breaking wave event on September 30th, 2012. The velocity shows comb-like structures (7:10 to 7:40) a downward motion of about 3 m/s and next to it an updraft of about 4 m/s. The fall speed of the small

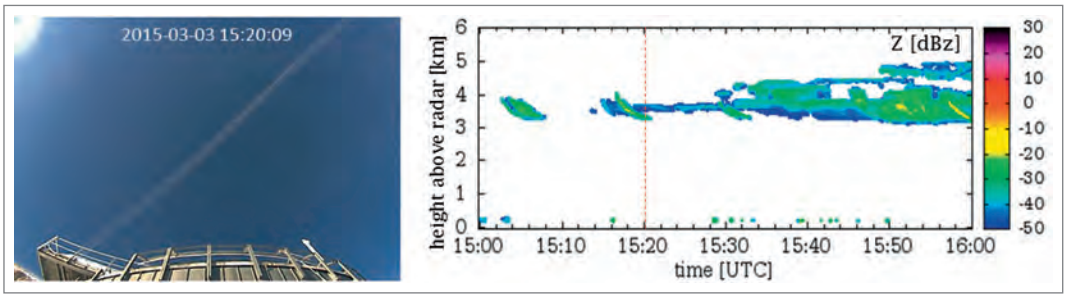

Fig. 6: Observation of a contrail by vertical looking camera (left) and cloud radar with a time-height display of reflectivity (right) on 3rd March 2015; the dashed orange line indicates the time of the photo by the automatic camera.

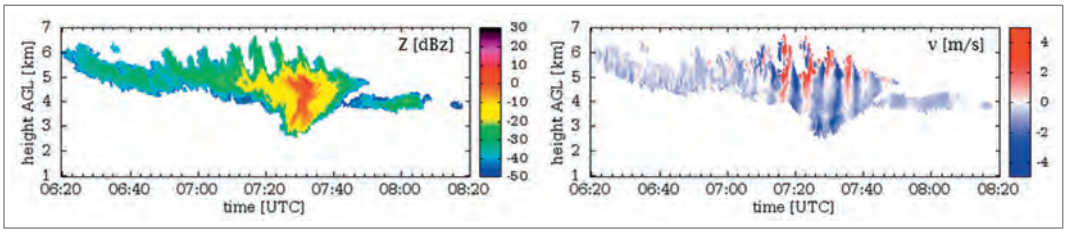

Fig. 7: Time-height cross-sections of reflectivity (left) and Doppler velocity (right) of a breaking wave event on 30th September 2012.

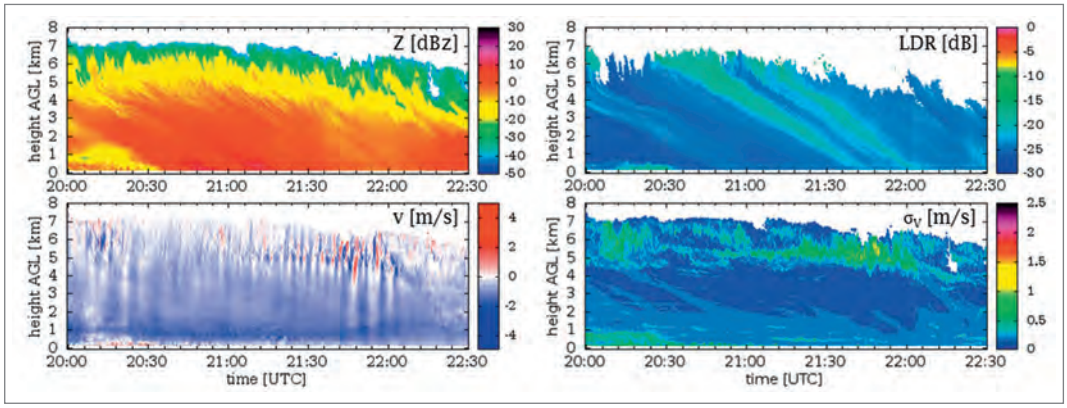

Fig. 8: Time-height cross-sections of reflectivity (upper left), linear depolarization ratio (upper right), Doppler velocity (lower left), and spectral width (lower right) of a fall streak event on 28th November 2012.

ice particles at that height is negligible (< 0.5 m/s). The breaking of waves is probably caused by strong wind shear at an inversion layer at about 9.5 km MSL (≈ 6.8 km above radar). The Innsbruck radio sounding from 3 UTC indicates horizontal winds with 21 m/s at 5 km and 39 m/s at 8 km above radar. Wind direction was 244° and 220°, respectively.

The third example is an event with fall streaks observed in snow. On November 28th, 2012 a homogeneous, about 7 km deep cloud layer with snowfall at ground was observed (Fig. 8). The time-height cross-section of reflectivity shows some diagonal structures which are related to fall streaks, when parcels of hydrometeors with enhanced reflectivity are falling down. At a time-height cross-section, the parcels can be seen first at cloud top and then later at the bottom. The signature of the fall streaks is more dominant in the linear depolarization ratio *LDR* (see Fig. 8, upper right). While *LDR* is about –25 dB outside the streaks it is about –15 dB within the streaks. This indicates larger and more irregular shaped particles with an unstable falling behavior. The main reason for the initiation of the streaks with enhanced *LDR* remains unclear. Doppler velocity shows up- and down-drafts at cloud top, there might be wind shear at that height. The enhanced turbulence in this upper region of the cloud is also seen in the spectral width (Fig. 8, lower left). Another possible explanation is the disturbances by aircraft, causing additional turbulence, humidity, and aerosol particles which in turn will initiate a different kind of ice particles.

5

5.3.1.3 Retrieval of Cloud Properties

Cloud physicists do prefer quantities which are related to cloud microphysics. Here we will show how radar parameters can be used to derive quantities like mean diameter of the particles and the ice water content.

A procedure to retrieve mean diameter from vertical pointing cloud radar was proposed by Matrosov et al. (2002). They use an empirical relation between mean diameter D_0 and fall velocity V_t

$$D_0 = 9 \cdot 10^{-4}\, V_t^3 - 6.6 \cdot 10^{-2}\, V_t^2 + 6.2\, V_t - 9.7 \tag{8}$$

with $V_t \geq 0.06$ m s^{-1}. From D_0 the ice water content IWC can be retrieved using a relation suggested by Atlas et al. (1995)

$$IWC = \frac{Z}{G \cdot D_0^3} \tag{9}$$

with Z in mm^6 m^{-3}, IWC in g m^{-3}, and D_0 in µm. G is a coefficient which depends on the bulk density, the shape and the particle size distribution.

The disadvantage using this approach at Schneefernerhaus is the occurrence of large vertical air motions which can be hardly corrected with the required precision. An alternative approach was suggested by Protat et al. (2007). They suggest using reflectivity and ambient temperature

$$\log(IWC) = 0.000372\, Z_{dBz} T + 0.0782\, Z_{dBz} - 0.0153\, T - 1.54 \tag{10}$$

with Z_{dBz} in dBz and temperature T in °C; or alternatively using only reflectivity if temperature is not available

$$IWC = 0.082\, z^{0.554} \tag{11}$$

Examples of the retrieval will be shown in section 5.3.2.2.

5.3.1.4 Retrieval of Vertical Velocity in Rain

As mentioned above in section 5.2.1.3 and 5.2.2.2, the measured Doppler velocity of a vertically pointing radar is the sum of the terminal fall velocity of the particles and the vertical air motion. Hauser and Amayenc (1981) suggested a method to retrieve rain drop size parameterization and vertical air motion. Assuming an exponential rain drop size distribution $n(D) = N_0\, e^{-\lambda D}$, the parameters N_0 as the hypothetical number of drops with diameter 0, the slope λ of the distribution, and the vertical air motion will iteratively be estimated until the difference between measured and estimated reflectivity (from N_0 and λ) is minimized.

The number of cases where this algorithm can be applied to MRR observations at Schneefernerhaus is limited since a sufficient thick rain layer (> 300 m) is fairly rare at the site. Fig. 9 shows two examples for the retrieval of the vertical air motion using a similar method proposed by Rogers (1964). On August 20th, 2016 mainly updrafts are observed, while on August 5th, 2016

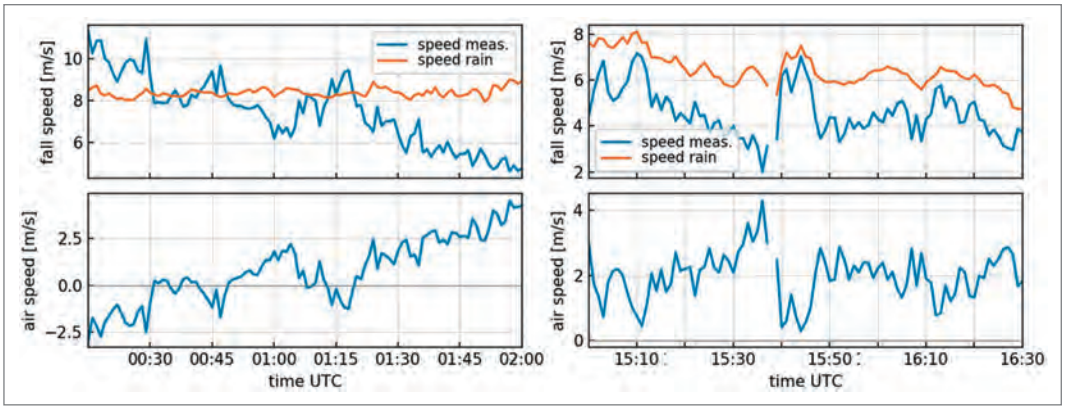

Fig. 9: Measured Doppler velocity (blue line – top figure) and retrieved vertical air motion (blue line – bottom figure) as well as fall velocity of the rain drop size distribution (orange line – top figure) for two events. Left: 5th August 2016; right: 20th August 2016. After Stucke (2017).

up- and downdrafts can be seen. The observations seem plausible considering the airflow on those days. Unfortunately, no independent verification for the retrieval of vertical air motion above UFS is available for these cases.

5.3.2 Evaluation of Satellite Observations with Radar at UFS

While the cloud radar and the micro rain radar provide high resolution data on a local vertical profile, satellite observations are used to provide information on a global or hemispheric scale. Satellites often only observe the top of the clouds and depending on the observation technique, the structure of the clouds and precipitation information can only be partly retrieved. Here we will show two examples, one using the polar orbiting cloud radar onboard CloudSat (Stephens et al., 2002), and a second example using the geostationary Meteosat Second Generation SEVIRI imager (Schmetz et al., 2002).

5.3.2.1 CloudSat Observations

Polar orbiting satellites like CloudSat, equipped with a nadir pointing W-band (wavelength 3.2 mm) cloud radar, or Calipso (equipped with lidar) very seldom pass directly over a specific site like the Schneefernerhaus. In addition, for the evaluation of cloud measurements, clouds have to be present during the short visiting time. To increase the sample number, all passes within 15 km have been used for the evaluation presented here. However, it has to be considered that due to the large inhomogeneity of the terrain, different types of clouds might be compared within the CloudSat footprint (diameter 1.2 km) and by the MIRA36 radar measuring only directly above UFS.

Fig. 10 shows a comparison of cloud properties and averaged reflectivity profiles for both cloud radars observed from 2012 to 2015. Only measurements above 3 km MSL have been considered for both systems in order to avoid disturbances due to surface reflections in the CloudSat data. The CloudSat radar is less sensitive compared to the MIRA36 radar. The reflectivity distribution and the averaged profiles agree very well, the difference is only 0.8 dB. The CloudSat radar is highly accurately calibrated using the well-known sea surface reflection (Kollias et al., 2019). The MIRA36 is calibrated by the manufacturer, a continuous independent calibration at the site is challenging because the radar beam cannot be directed towards a target whose scattering

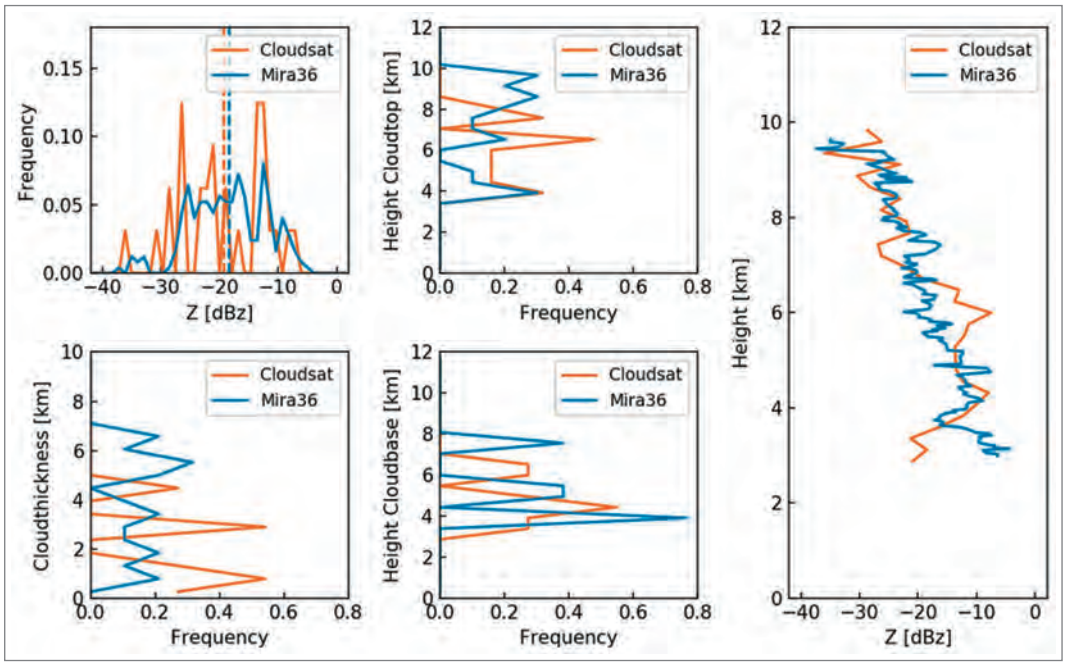

Fig. 10: CloudSat (orange) and UFS-MIRA (blue) observations of cloud properties for the years 2012–2015. Top left: frequency distribution of reflectivities; Top center: frequency distribution of cloud top height; bottom left: frequency distribution of cloud thickness; bottom center: frequency distribution of cloud base height. Right: averaged reflectivity profiles.

properties are well known. The lower reflectivity values for the CloudSat radar profile between 3 and 3.7 km are most likely caused by attenuation in thick clouds. The cloud properties show that the lower sensitivity of the CloudSat radar has limitations observing high thin cirrus clouds.

5.3.2.2 Meteosat SEVIRI Observations

The geostationary observations of SEVIRI allow for a continuous observation of cloud properties. For a comparison we select the ice water path (*IWP*) which is the vertical integral of *IWC*. SEVIRI resolution is about 3.2×5.5 km^2 over the Schneefernerhaus. Nine values of *IWP* over an area of 3 by 3 pixels (app. 10×16 km^2) were estimated using the APICS algorithm (Bugliaro et al., 2011). The *IWP* was then compared to the vertically integrated *IWC* derived from the MIRA36 measurements. The algorithms described by equations (9) to (11) were applied for the MIRA36 measurements.

Fig. 11 shows the comparison for two events, one in June 2014 and one in January 2015. In general, there is an agreement between the radar algorithms using reflectivity only (*IWP-Z*; Eq. 11) and temperature and reflectivity (*IWP-Z-T*; Eq. 10), whereas the algorithm using vertical velocity (*IWP-Z-VEL*; Eq. 9) shows a large scatter. This is attributed to the unknown vertical air motion over the site. Obviously, during times where the vertical air motion was small, the *IWP-Z-VEL* algorithm agrees well with the other two algorithms. The comparison to the APICS algorithm shows varying agreement. This mainly depends on the structure of the clouds and precipitation. The SEVIRI retrieval is dominated by information originating from the cloud top area due its limited capability to penetrate thicker clouds. The lower part of thick clouds or precipitation is not seen by SEVIRI.

The measurements on June 29th, 2014 show a nearly homogeneous cloud layer with precipitation, the *IWP* is overestimated by SEVIRI, especially during the time when rain was observed at Schneefernerhaus (approximately until 12:30). Only minor horizontal variation is visible within the 3×3 SEVIRI pixels. On January 16th, 2015 a deep cirrus layer was observed. The 3×3 SEVIRI pixels show large variation, this is an indication that there was high spatial variation in the cloud layer and the measurements by the radar might not be representative for the area seen by SEVIRI.

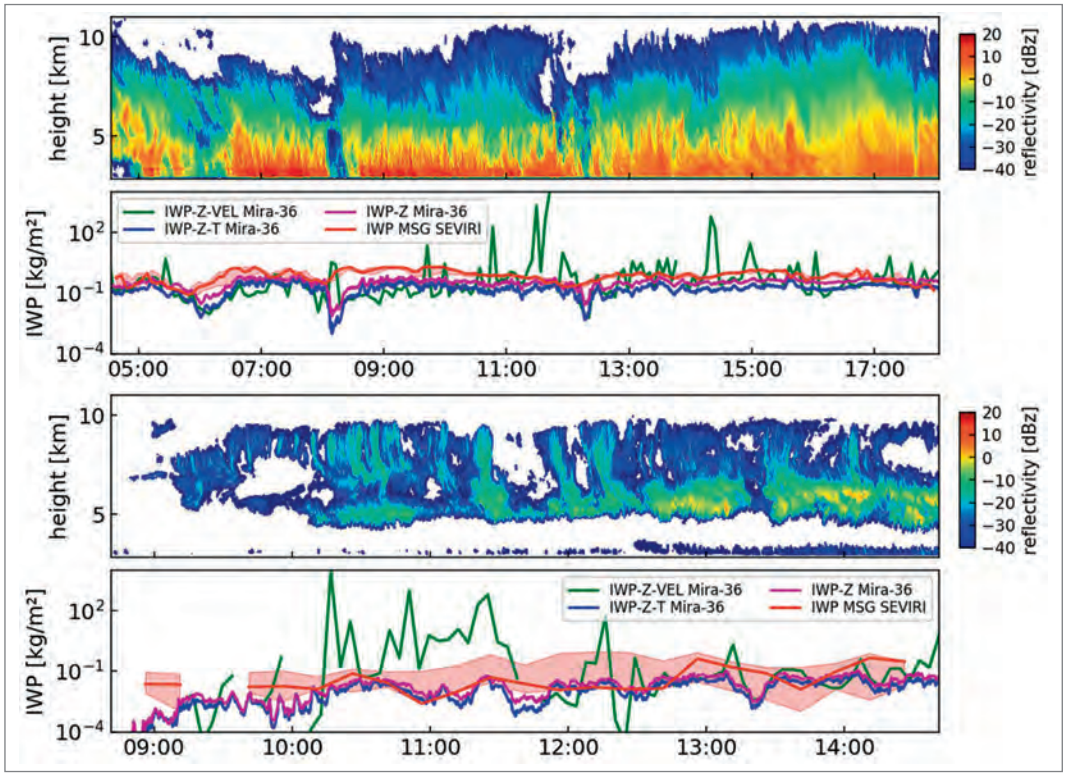

Fig. 11: Reflectivity observations by MIRA36 and retrieved ice-water-path (IWP) for 29 June 2014 (top 2 rows) and 16 January 2015 (bottom 2 rows). IWP estimated from MIRA by 3 techniques (see text) and from Meteosat SEVIRI. Red line is pixel over Schneefernerhaus; shaded area is range of IWP over 3×3 pixels.

5.3.3 The TOSCA Campaign

The TOSCA campaign (**T**owards an **O**ptimal estimation-based **S**now **C**haracterization **A**lgorithm) took place at Schneefernerhaus during the winter 2007/2008 and 2008/2009. Details can be found in Löhnert et al. (2011). The motivation for the campaign was a synergistic combination of state-of-the-art remote sensing instruments with the goal to develop a modular optimal-estimation algorithm and to evaluate the potential for deriving columnar snow microphysics. The success of running the first cloud radar at the UFS was the main motivation to permanently install such a radar at UFS. During TOSCA, the cloud radar data were combined with ceilometer and the two permanently installed microwave radiometers (Humidity and Temperature Profiler HATPRO and Dual Polarization Radiometer DPR) providing observations in the frequency range from 22 up to 150 GHz, which is similar to space-borne microwave sensors. In addition, in-situ sensor for the size, fall velocity and shape of the snowflakes were installed at the UFS. Radar and radiometer are often combined because the radar provides profile information while the radiometer is able to better quantify the integrated quantities in the atmospheric column (e. g., ice water path, liquid water path, water vapor integral). For snow and ice processes, the presence of supercooled liquid water (liquid water can be found down to –38 °C in the atmosphere) plays a central role. While it is very hard to detect it in radar observations, the radiometers are extremely sensitive to it, especially at the higher frequencies provided at the UFS. In general, the radiometers are only sensitive to scattering by ice and snow particles at frequencies larger than 90 GHz, which makes them well suited to constrain the amount of liquid water in comparison to ice.

One main outcome of TOSCA was that supercooled liquid water is almost always present in snowfall at UFS and its amounts could be quantified and linked to other parameters such as temperature, for the first time (Löhnert et al., 2011). The unique DPR radiometer, further provided the first observations of snow scattering signals in ground-based radiometers – an effect, which was so far only been known for space-borne radiometers. This confirmed the principal potential of ground-based radiometers to constrain snowfall properties (Kneifel et al., 2010). The polarimetric observations of the DPR further confirmed that snowflakes fall with a preferential orientation – a question which was debated for a long time in the snowfall remote sensing community (Xie et al., 2012).

The long-term combined radar-radiometer measurements also provided valuable data to develop new absorption models for supercooled liquid water (Kneifel et al., 2014; Turner et al., 2016), which are key components for global satellite retrievals. The parallel observations of the MIRA36 cloud radar and the MRR also provided a dataset to develop a new algorithm to measure snowfall with the MRR (Kneifel et al., 2011; Maahn and Kollias, 2012). These studies triggered the use of MRRs in other remote areas such as the Arctic and Antarctic for the so far very difficult estimation of snowfall – the main source term for the polar ice sheet mass balance.

An interesting feature found in the in-situ measurements (2D-video disdrometer; c. f. Fig. 7 in Löhnert et al., 2011) during TOSCA was that maximum snow particle size D_{max} seems to be temperature independent – except for the temperature range between –10 and –15 °C where large snow crystals occur more frequent. In this temperature range, the super saturation over ice with respect to liquid water reaches its maximum value so that the Wegener-Bergeron-Findeisen process, i. e. the transformation of liquid drops to ice crystals via gas phase, will be more effective. Also, snow crystals are mostly of dendritic structure in this temperature range. Both conditions are preferable for the fast and effective growth by aggregation of snow crystals in this "secondary growth region".

5.3.4 Cloudnet

Cloudnet is an European initiative (Illingworth et al., 2007) to provide a systematic evaluation of clouds and precipitation in numerical weather prediction models. The efforts to improve the representation of clouds and precipitation in forecast models have been limited by the difficulty to make appropriate and accurate observations. Cloud parameters used in models differ from the parameters which are available from observations; thus, a common basis needs to be defined for comparison and evaluation. Another fact is that often evaluations are performed based on case studies; however, to improve forecast models a long-term evaluation is needed. To achieve a suitable evaluation, the Cloudnet project was established. It involves instrument

5

operators as well as developers of forecast models all across Europe. A number of already existing ground based remote sensing sites were brought together for this purpose. These sites are operated now since many years in order to gain statistics unaffected by seasonality. Moreover, the Cloudnet community was able to develop robust algorithms for quality control and retrieval of microphysical quantities of clouds and precipitation.

Cloudnet is embedded in the European ACTRIS (Aerosols, Clouds and Trace gases Research Infrastructure) project and in Germany supported by the HD(CP)^2 (High Definition Clouds and Precipitation for advancing Climate Prediction) project. Currently, about 10 sites contribute to Cloudnet together with additional non-European sites equipped with similar instrumentation. The Meteorological Institute (MIM) at Munich University (LMU) and the UFS Schneefernerhaus are members of Cloudnet since 2018. Processing of UFS data is performed at MIM. Real-time observations and model forecasts together with daily and monthly quicklooks and statistics of model performance are provided at the Cloudnet web site (http://cloudnet.fmi.fi/).

The core instruments at MIM and UFS are the high power and sensitive MIRA36 cloud radar, a low-power lidar – the ceilometer, and the multi-wavelength microwave radiometer HATPRO. The radar provides detailed information on the vertical structure of the clouds. The ceilometer is used to identify the cloud base – mainly of water clouds – more accurately. If attenuation by cloud particles is not too strong, profiles of the lidar backscatter signal are available in the cloud. The microwave radiometer provides vertical profiles of temperature and humidity, and integrated quantities like liquid water path (LWP) and vertical integrated water vapor (IWV).

The Cloudnet processing chain includes in a first step a target classification using the fact that the radar is sensitive to large particles like rain, drizzle, ice particles, while the lidar is sensitive to smaller particles like cloud droplets and aerosols. Quality control of the radar data includes an attenuation correction for gaseous attenuation (water vapor and oxygen) as well as for liquid water using information from the microwave radiometer. Doppler velocity helps to distinguish between snow and rain. Higher level Cloudnet products comprise liquid water content (LWC), ice water content (IWC), and drizzle parameters. Fig. 12 shows a sample of the input measure-

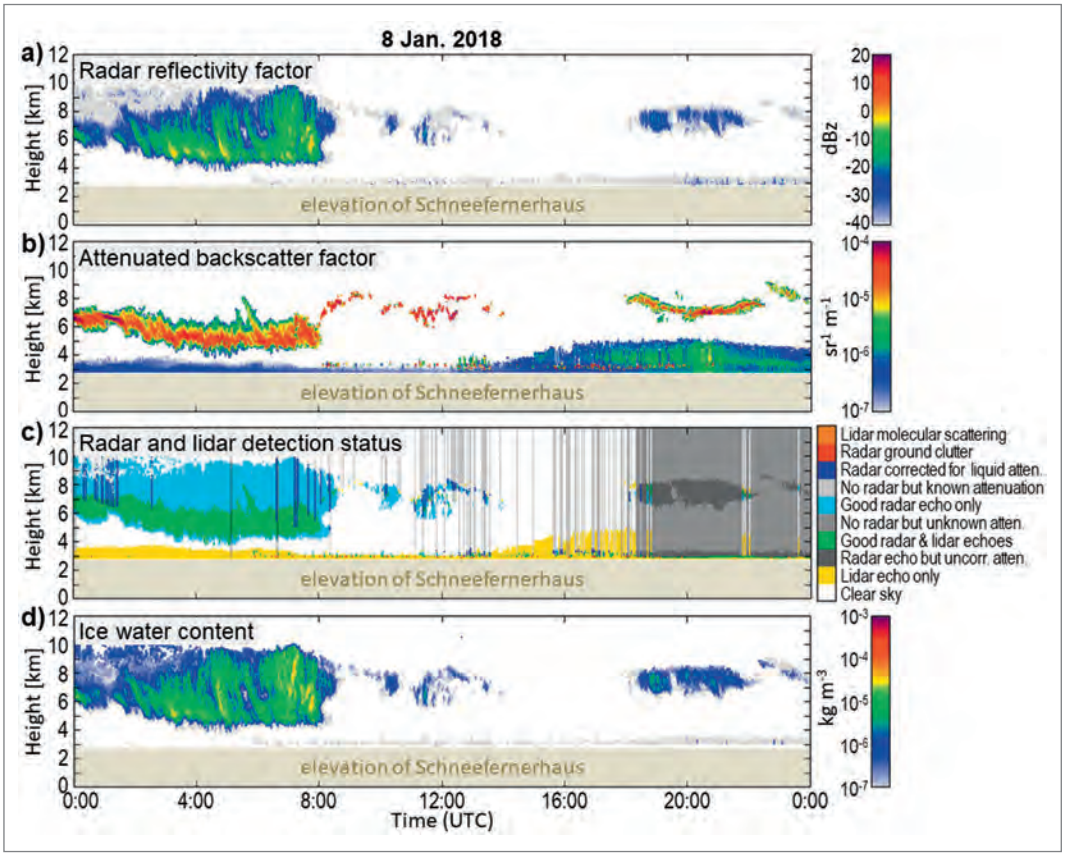

Fig. 12: Cloudnet products: Measurements with cloud radar (a) and ceilometer (b) at UFS Schneefernerhaus on 8th January 2018. The radar and lidar status is shown in c), the retrieved ice water content (IWC) in d).

ments and the retrieved quantities. It can be clearly observed that the lidar partly penetrates into the cloud and there is an overlap between both instruments. Future activities will also include the evaluation of satellite observations of clouds and precipitation.

5.4 Summary and Conclusions

Meteorological radar is an essential tool for research, diagnostic, and nowcasting of clouds and precipitation. Modern radar systems provide a number of parameters like reflectivity, Doppler velocity, or dual-polarization products. The parameters can be used to study intensity, motion, or habits of cloud and precipitation particles.

At UFS Schneefernerhaus a MIRA36 cloud radar (wavelength 8 mm) and a micro-rain-radar (MRR, wavelength 12 mm) have been installed. The cloud radar has been operated since the end of 2011, a similar system was installed already 2008–2009 during the TOSCA campaign; the MRR has been operated since the beginning of 2008. The long-term operation of the radars allows for deriving detailed statistics of clouds and precipitation above UFS Schneefernerhaus. Clouds cover the sky over Schneefernerhaus about half of the time and are observed up to 12.5 km above sea-level. Some examples of measurements of contrail cirrus or fall streaks were given to show the benefit from radar observations.

Both radar systems operate in a vertical pointing mode and provide cloud and precipitation structures above Schneefernerhaus. The cloud radar provides data with high temporal (10 seconds) and spatial (30 m) resolution at a beam width of 0.6° (e. g. diameter of 50 m at a distance of 5 km). Both systems provide in real-time the Doppler spectra, a quantity which can be used to study the falling behavior and thus the habit of cloud and precipitation particles. One of the major challenges in the data evaluation is the high variability of the surrounding wind field, especially the vertical air motion. Fall speed of cloud particles is superimposed to the vertical air motion and turbulence. Algorithms have been developed which are able to account for these effects; however, they require prior knowledge of terminal fall speed and the particle size distribution.

The long-term operation of the radars and the synergy with lidar and microwave radiometer gives a unique possibility for the evaluation of cloud and precipitation microphysics in numerical weather prediction models or of satellite measurements of clouds and precipitation. The UFS is worldwide the only mountain site which provides now a decade-long remote sensing observations of clouds and precipitation using this comprehensive instrument combination. This allows for monitoring potential changes in clouds and precipitation in a warming climate which is expected to be particularly pronounced at higher altitudes. The European project Cloudnet is designed for the evaluation of several weather forecast models by long-term observations at a number of sites with similar instrumentation like the Schneefernerhaus. Together with a ceilometer as low-cost and robust lidar system and the microwave radiometer, the cloud radar is contributing to Cloudnet. The same constellation together with the algorithms provided by Cloudnet can also be used for the evaluation of satellite measurements. Polar orbiting satellites like CloudSat, Calipso, GPM, or the upcoming EarthCARE satellite provide measurements with radar and lidar which are comparable to the observations at Schneefernerhaus. Geostationary satellites like Meteosat provide a set of additional cloud parameters which can be used for further evaluations. Even though the spatial resolution of geostationary satellites is not sufficient to describe clouds in the complex orography of the Wetterstein massif, they help in understanding the temporal evolution and regional distribution of the cloud systems observed above Schneefernerhaus.

Acknowledgement

The MIRA36 cloud radar was provided through the funds of the developing project plan (EPP) 2008–2012 of the Bavarian State Ministry of the Environment. The support from the UFS team – especially Markus Neumann and Till Rehm – is greatly acknowledged, without their help and support the installation and operation of the instruments would be much more challenging and the long time series of continuous operation would not be possible. We also have to thank Matthias Bauer-Pfundstein from METEK GmbH for the support during the installation and operation of the cloud radar.

5

References

Acquistapace, C., S. Kneifel, U. Löhnert, P. Kollias, M. Maahn, and M. Bauer-Pfundstein, 2017: Optimizing observations of drizzle onset with millimeter-wavelength radars, *Atmos. Meas. Tech.*, **10**, 1783–1802, https://doi.org/10.5194/amt-10-1783-2017.

Atlas, D., S.Y. Matrosov, A.J. Heymsfield, M. Chou, and D.B. Wolff, 1995: Radar and radiation properties e clouds. *J. Appl. Meteor.,* **34**, 2329–2345, https://doi.org/10.1175/1520-0450(1995)034<2329:RARPOI>2.0.CO;2.

Atlas, D, R. Srivastava, and R. Sekhon, 1973: Doppler radar characteristics of precipitation at vertical incidence. Rev. Geophys. Space Phys., **11**, 1–35, https://doi.org/10.1029/RG011i001p00001.

Bringi, V.N., and V. Chandrasekar, 2001: *Polarimetric Doppler Weather Radar: Principles and Applications*. Cambridge University Press, 648 pp, https://doi.org/10.1017/CBO9780511541094.

Bugliaro, L., T. Zinner, C. Keil, B. Mayer, R. Hollmann, M. Reuter, and W. Thomas, 2011: Validation of cloud property retrievals with simulated satellite radiances: a case study for SEVIRI. *Atmos. Chem. Phys.*, **11**, 5603–5624, https://doi.org/10.5194/acp-11-5603-2011.

Fabry, F. (2015). *Radar Meteorology: Principles and Practice*. Cambridge: Cambridge University Press. https://doi.org/10.1017/CBO9781107707405.

Görsdorf, U., V. Lehmann, M. Bauer-Pfundstein, G. Peters, D. Vavriv, V. Vinogradov, and V. Volkov, 2015: A 35-GHz polarimetric Doppler radar for long-term observations of cloud parameters – description of system and data processing. *J. Atmos. Oceanic Technol.*, **32**, 675–690, https://doi.org/10.1175/JTECH-D-14-00066.1.

Häring, A., 2016: *Synergetic cloud observations with cloud radar and satellite instruments*. Master Thesis, Ludwig-Maximilians-Universität München, 69 pp. Available at https://elib.dlr.de/107232.

Illingworth, A.J., R.J. Hogan, E. O'Connor, D. Bouniol, M.E. Brooks, J. Delanoé, D.P. Donovan, J.D. Eastment, N. Gaussiat, J.W. Goddard, M. Haeffelin, H.K. Baltink, O.A. Krasnov, J. Pelon, J. Piriou, A. Protat, H.W. Russchenberg, A. Seifert, A.M. Tompkins, G. van Zadelhoff, F. Vinit, U. Willén, D.R. Wilson, and C.L. Wrench, 2007: Cloudnet: Continuous evaluation of cloud profiles in seven operational models using ground-based observations. *Bull. Amer. Meteor. Soc.,* **88**, 883–898, https://doi.org/10.1175/BAMS-88-6-883.

Illingworth, A.J., H.W. Barker, A. Beljaars, M. Ceccaldi, H. Chepfer, N. Clerbaux, J. Cole, J. Delanoë, C. Domenech, D.P. Donovan, S. Fukuda, M. Hirakata, R.J. Hogan, A. Huenerbein, P. Kollias, T. Kubota, T. Nakajima, T.Y. Nakajima, T. Nishizawa, Y. Ohno, H. Okamoto, R. Oki, K. Sato, M. Satoh, M.W. Shephard, A. Velázquez-Blázquez, U. Wandinger, T. Wehr, and G. van Zadelhoff, 2015: The EarthCARE satellite: The next step forward in global measurements of clouds, aerosols, precipitation, and radiation. *Bull. Amer. Meteor. Soc.,* **96**, 1311–1332, https://doi.org/10.1175/BAMS-D-12-00227.1.

Kneifel, S., U. Löhnert, A. Battaglia, S. Crewell, and D. Siebler, 2010: Snow scattering signals in ground-based passive microwave measurements. *J. Geophys. Res.*, **115**, D16214, https://doi.org/10.1029/2010JD013856.

Kneifel, S., M. Maahn, G. Peters, and C. Simmer, 2011: Observation of snowfall with a low-power FM-CW K-band radar (Micro Rain Radar). *Meteorol. Atmos. Phys.*, **113**, 75–87, https://doi.org/10.1007/s00703-011-0142-z.

Kneifel, S., B. Pospichal, L. von Terzi, T. Zinner, M. Puh, M. Hagen, B. Mayer, U. Löhnert, S. Crewell, 2021: Multi-year cloud and precipitation statistics observed with remote sensors at the high-altitude Environmental Research Station Schneefernerhaus in the German Alps. Meteorologische Zeitschrift, 31, 69–86. https://doi:10.1127/metz/2021/1099.

Kneifel, S., S. Redl, E. Orlandi, U. Loehnert, M.P. Cadeddu, D.D. Turner, and M.-T. Chen, 2014: Absorption properties of supercooled liquid water between 31 and 225 GHz: Evaluation of absorption models using ground-based observations. *J. Appl. Meteor. Climatol.*, **53**, 1028–1045, https://doi.org/10.1175/JAMC-D-13-0214.1.

Kollias, P., B. Puigdomènech Treserras, and A. Protat, 2019: Calibration of the 2007–2017 record of ARM Cloud Radar Observations using CloudSat, Atmos. Meas. Tech., **12**, 4949–4964, https://doi.org/10.5194/amt-12-4949-2019.

Kollias, P., J. Rémillard, E. Luke, and W. Szyrmer, 2011: Cloud radar Doppler spectra in drizzling stratiform clouds: 1. Forward modeling and remote sensing applications, *J. Geophys. Res.*, **116**, D13201, https://doi.org/10.1029/2010JD015237.

Löffler-Mang, M. and J. Joss, 2000: An optical disdrometer for measuring size and velocity of hydrometeors. *J. Atmos. Ocean. Tech.*, **17**, 130–139, https://doi.org/10.1175/1520-0426(2000)017<0130:AODFMS>2.0.CO;2.

Löhnert, U., S. Kneifel, A. Battaglia, M. Hagen, L. Hirsch, and S. Crewell, 2011: A multisensor approach toward a better understanding of snowfall microphysics: The TOSCA project. *Bull. Amer. Meteorol. Soc.*, **92**, 613–628, https://doi.org/10.1175/2010bams2909.1.

Maahn, M. and P. Kollias, 2012: Improved Micro Rain Radar snow measurements using Doppler spectra post-processing, *Atmos. Meas. Tech.*, **5**, 2661–2673, https://doi.org/10.5194/amt-5-2661-2012.

Matrosov, S.Y., A.V. Korolev, and A. J. Heymsfield, 2002: profiling cloud ice mass and particle characteristic size from Doppler radar measurements. *J. Atmos. Oceanic Technol.,* **19**, 1003–1018, https://doi.org/10.1175/1520-0426(2002)019<1003:PCIMAP>2.0.CO;2.

Mech, M., E. Orlandi, S. Crewell, F. Ament, L. Hirsch, M. Hagen, G. Peters, and B. Stevens, 2014: HAMP – the microwave package on the High Altitude and LOng range research aircraft (HALO), *Atmos. Meas. Tech.*, **7**, 4539–4553, https://doi.org/10.5194/amt-7-4539-2014.

Melchionna, S., M. Bauer, and G. Peters, 2008: A new algorithm for the extraction of cloud parameters using multipeak analysis of cloud radar data – first application and preliminary results. *Meteorol. Z.*, **17**, 613–620, https://doi.org/10.1127/0941-2948/2008/0322.

Peters, G., B. Fischer, T. Andersson, 2002: Rain observations with a vertically looking Micro Rain Radar (MRR). *Boreal Environ. Res.*, **7**, 353–362.

Protat, A., J. Delanoë, D. Bouniol, A. J. Heymsfield, A. Bansemer, and P. Brown, 2007: evaluation of ice water content retrievals from cloud radar reflectivity and temperature using a large airborne in situ microphysical database. *J. Appl. Meteor. Climatol.*, **46**, 557–572, https://doi.org/10.1175/JAM2488.1.

Rogers, R. R., 1964: An extension of the *Z-R* relationship for Doppler radar. *Proc. 11 Weather Radar Conf.*, Boulder, Amer. Meteor. Soc., 158–169.

Schmetz, J., P. Pili, S. Tjemkes, D. Just, J. Kerkmann, S. Rota, and A. Ratier, 2002: An Introduction to Meteosat Second Generation (MSG). *Bull. Amer. Meteor. Soc.*, **83**, 977–992, https://doi.org/10.1175/1520-0477(2002)083%3C0977:AITMSG%3E2.3.CO;2.

Skolnik, M. I., 2008: *Radar Handbook*. 3rd ed. McGraw-Hill Professional, 1350 pp.

Stephens, G. L., D. G. Vane, R. J. Boain, G. G. Mace, K. Sassen, Z.Wang, A. J. Illingworth, E. J. O'Connor, W. B. Rossow, S. L. Durden, S. D. Miller, R.T. Austin, A. Benedetti, C. Mitrescu, and the CloudSat Science Team, 2002: The CloudSat mission and the A-Train. *Bull. Amer. Meteor. Soc.*, **83**, 1771–1790, https://doi.org/10.1175/BAMS-83-12-1771.

Stucke, I., 2017: *Bestimmung der Vertikalgeschwindigkeit und des Tropfenspektrums aus Dopplermessungen mit einem vertikal gerichteten Mikro-Regen-Radar*. Bachelor Thesis, Leopold-Franzens-Universität Innsbruck, 61 pp.

Turner, D. D., S. Kneifel, and M. P. Cadeddu, 2016: An improved liquid water absorption model in the microwave for supercooled liquid water clouds, *J. Atmos. Oceanic Tech.*, **33**, 33–44, https://doi.org/10.1175/JTECH-D-15-0074.1.

Xie, X., U. Löhnert, S. Kneifel, and S. Crewell, 2012: Snow particle orientation observed by ground-based microwave radiometry, *J. Geophys. Res.*, **117**, D02206, https://doi.org/10.1029/2011JD016369.